PCCP

PAPER

View Article Online
View Journal | View Issue

Cite this: *Phys. Chem. Chem. Phys.*, 2017, **19**, 3046

Complexation of short ds RNA/DNA oligonucleotides with Gemini micelles: a time resolved SAXS and computational study†

Sara Falsini,[a] Emanuela Di Cola,[b] Martin In,[c] Maria Giordani,[d] Stefano Borocci[de] and Sandra Ristori[f]

Gene therapy is based on nucleic acid delivery to pathogenic cells in order to modulate their gene expression. The most used non viral vectors are lipid-based nanoaggregates, which are safer than viral carriers and have been shown to assemble easily with both DNA and RNA. However, the transfection efficiency of non viral carriers still needs to be improved before intensive practise in clinical trials can be implemented. For this purpose, the in depth characterization of the complexes formed by nucleic acids and their transporters is of great relevance. In particular, information on the structure and assembly mechanism can be useful to improve our general knowledge of these artificial transfection agents. In this paper, the complexation mechanism of short interfering RNA and DNA molecules (siRNA and siDNA, respectively) with cationic micelles is investigated by combining small angle X-ray scattering experiments and molecular dynamics simulations. Micelles were obtained by Gemini surfactants with different spacer lengths (12-3-12, 12-6-12). The siRNA and siDNA used were double strand molecules characterized by the same length and homologous sequence, in order to perform a close comparison. We showed that complexes appear in solution immediately after mixing and, therefore, the investigation of complex formation requires fast experimental techniques, such as time resolved synchrotron SAXS (Tr-SAXS). The obtained systems had internal arrangement constituted by layers of squeezed micelles alternating the nucleic acids. Both SAXS and MD analyses allowed us to evaluate the mean size of complexes in the range of a few nanometers, with looser and less ordered stacking for the DNA containing aggregates.

Received 21st September 2016,
Accepted 19th December 2016

DOI: 10.1039/c6cp06475b

www.rsc.org/pccp

Introduction

The development of therapeutic technologies based on nucleic acid has recently intensified, due to the potentiality that they bear for overcoming the drawbacks of conventional treatments, such as immunogenic effects. In particular, RNA interference is a most promising approach for biomedical applications.[1,2] This approach consists in the post-transcriptional gene silencing, mediated by small double stranded RNA (small interfering RNA, siRNA).[3] The exogenous introduction of siRNA into human cells triggers the cleavage of mRNA with a complementary sequence, causing the knockdown of a specific gene.[4] Therefore, siRNA can be exploited as a tool in gene therapy for its ability to sequence specific gene silencing.[5] Not only siRNA, but also synthetic double strand DNA molecules (of ~30 bp, siDNA) are able to activate an interfering pathway into human cells. In contrast to siRNAs, siDNAs interfere with the signalling of DNA double-strand break (DSB) repair and are able to hinder the DNA damage response, inhibiting DNA repair.[6] siDNA could thus be exploited to inhibit DNA repair into cancer cells and sensitize these cells to genotoxic therapies which are rejected under normal conditions.[7,8]

One of the major challenges in gene therapy is the development of non-viral platforms for oligonucleotides to obtain efficient delivery systems. Currently, the most promising non-viral vectors are cationic self-assembled nanoaggregates, such as liposomes or micelles.[9–11] When vectors are mixed with oligonucleotides or

[a] *Department of Chemistry "Ugo Shiff" & CSGI, University of Florence, Via della Lastruccia 3, 50019 Sesto Fiorentino, FI, Italy*
[b] *European Synchrotron Radiation Facility (ESRF)71 Avenue des martyrs 38000, Grenoble, France*
[c] *Laboratoire Charles Coloumb, UMR, 5221 CNRS-UM, Place Eugène Bataillon, F-34095 Montpellier Cedex 05, France*
[d] *CNR-Istituto di Metodologie Chimiche, Area della Ricerca di Roma 1, Via Salaria km 29300, 00015 Monterotondo RM, Italy*
[e] *Dipartimento per la Innovazione nei Sistemi Biologici, Agroalimentari e Forestali (DIBAF), Università degli Studi della Tuscia, Largo dell'Università, snc 01100, Viterbo, Italy*
[f] *Dipartimento di Scienze della Terra, Università di Firenze, Via La Pira 4, 50121, Firenze, Italy*

† Electronic supplementary information (ESI) available. See DOI: 10.1039/c6cp06475b

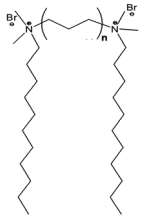

Fig. 1 Molecular structure of Gemini surfactants.

plasmids, new aggregates of nano- and micro-scale sizes are formed in solution. In particular, it has been observed that the structure of certain lipid components, such as Gemini amphiphiles, might strongly affect the complexation of ODN molecules. In fact, in Gemini two polar heads are joined by a spacer, and the nature and length of this covalent link control the interaction with the ODN and its compaction.[12] The study of the complexation process and the structural properties of the ensuing aggregates are of fundamental importance to understand the mechanisms of delivering and transfection. For this purpose it has been shown that time resolved SAXS (Tr-SAXS) experiments offer the opportunity to obtain information on the size and shape of complexes,[13] and to study their internal reorganization at a 10 ms time scale. The results of such experiments can be combined with molecular dynamics (MD) simulations to provide detailed information on the complexation process, at the atomistic level and at the 10–100 ns timescale. MD simulations are used as a "computational microscope",[14] to study at the atomic level with picoseconds-scale time resolution the structure, organization and dynamics of biomacromolecules and molecular complexes.[15] Moreover, MD simulations provide structural and dynamics features of molecular systems which cannot be easily probed with experimental techniques.[16] Indeed, all-atoms MD simulations of oligonucleotides (ODNs) with nanoaggregates such as dendrimers,[17] gold nanoparticles[18] and micelles[19,20] have been used to investigate the structure and strength of ODN/nanoaggregate interactions.

Here we studied the structural evolution of complexes formed by double strand oligonucleotides (siRNA as well as siDNA) with micelles of dimeric cationic surfactants *i.e.* Gemini bis (quaternary ammonium) bromide with variable spacer lengths, 12-3-12 and 12-6-12 (Fig. 1), combining Tr-SAXS experiments and all-atom MD simulations.

In order to have a meaningful comparison, the chosen RNA and DNA had the following homolog sequence:

sense: 5′ GAUAAAGGAGCGAACCCACUU 3′
antisense 3′ UUCUAUUUCCUCGCUUGGGUG 5′
sense: 5′ GATAAAGGAGCGAACCCACTT3′
antisense 3′ TTCTAT T TCCTCGC T TGGGTG 5′

Materials and methods

(a) SAXS experiments

Tr-SAXS was performed at the high brilliance SAXS beamline ID02 of the European Synchrotron Radiation Facility (Grenoble, France). The range of scattering vector q covered was 0.080–3.8 nm^{-1} with a sample-detector distance of 1.5 m. q is defined as:

$$q = \frac{4\pi}{\lambda}\sin\frac{\theta}{2}$$

where θ is the scattering angle and λ the X-ray wavelength (λ = 0.1 nm).

Complexes between oligonucleotides and micelles were prepared by mixing equal volumes (100 μL) of MilliQ water solutions of cationic surfactants and ODNs at the appropriate concentration to obtain two charge ratios below and above neutralization: ([−]/[+])CR = 0.75 and CR = 1.25. In these experiments, all systems contained a fixed amount of surfactant, *i.e.* 1.25×10^{-3} M, higher than the critical micelle concentration, CMC.[21]

For the kinetic runs, the surfactant and ODN solutions were mixed using a stopped flow device (SFM-400), as described elsewhere.[13] The flow rate was 5 mL s^{-1} and the acquisition time was 10 ms. Each experiment consisted of 80–100 frames, collected in three different time groups: each 0.15 s, each 2–3 s and each 40–60 s. Static experiments on micelles were performed with a sample to detector distance of 0.8 m (0.1 $nm^{-1} < q < 8$ nm^{-1}) in a flow through the capillary of 2 mm diameter to ensure an accurate subtraction of the background (buffer solution) and negligible beam damage of the samples. In this case, the acquisition time was 0.1 or 0.2 s.

The scattering patterns $I(q)$ were normalized to absolute intensity after applying standard corrections for spatial homogeneity and linearity. Each measurement was repeated at least twice, to ensure reproducibility.

(b) Molecular dynamics simulations

All molecular dynamics simulations were performed by using GROMACS 5.0.4 packages[22] in combination with the CHARMM36[23,24] force field for nucleic acids and CHARMM36 UA[25] for Gemini surfactants.

The 21 base-pair double-stranded siRNA (form A) and siDNA (form B) models were generated by using the Nucleic Acid Builder (NAB)[26] *via* the make-na server (http://casegroup.rutgers.edu/).

The initial structure of nucleic acid (siRNA and siDNA) was equilibrated by 20 ns molecular dynamics simulations, under constant pressure–constant temperature conditions (*NPT* ensemble), before the simulation with micelles of Gemini surfactants. The nucleic acid was solvated with water molecules in a rectangular box of 7.0 × 7.0 × 9.0 nm^3 and 40 sodium ions were used to neutralize the negative charges of nucleic acid. The energy was minimized and the molecular systems were equilibrated with 100 ps of MD simulations with the position restraints on the nucleic acids (1000 kJ mol^{-1} nm^2) followed by 20 ns of unrestrained MD simulations.

Micelles of Gemini, 12-3-12 and 12-6-12, were simulated as follows: 27 molecules of the Gemini surfactant were placed randomly in a cubic box of 8.5 × 8.5 × 8.5 nm^3 and solvated with water. The positive charges of the surfactant molecules were neutralized by replacing 54 solvent molecules with bromide ions. The energy was minimized and the system was equilibrated

with 100 ps of MD with position restraints on the surfactant molecules followed by 60 ns of unrestrained MD simulations.

The equilibrated nucleic acids and micelles were used to build the initial configuration of the ODN/micelle systems.

In a rectangular box of 10.3 × 7.8 × 9.7 nm^3 the micelle of Gemini (12-6-12 and 12-3-12) was placed in proximity of nucleic acid, with a distance of 4.0 nm between the centre of mass of the micelle and the centre of mass of nucleic acid (siRNA or siDNA). The systems were solvated and the electric charges were neutralised with 54 bromide ions and 40 sodium ions. The resulting systems were minimized and equilibrated using 100 ps of MD simulations with position restraints on the ODNs and surfactant atoms followed by 100 ns of unrestrained MD simulations.

The structure of the monomeric complex ODN/micelle, obtained after 80 and 100 ns of MD simulations, was used to build the initial configuration for the simulation of the dimeric complexes. For each system, composed of two molecules of nucleic acid (siRNA or siDNA) and two micellar aggregates, the complex at 100 ns was placed in proximity of the complex at 80 ns at a distance of 5.0 nm between the centre of mass of the micelles. Each dimeric system was solvated in a rectangular box of 10.0 × 12.0 × 10.0 nm^3 and the electric charges were neutralized with 108 bromide ions and 80 sodium ions. The energy of each system was minimized and the molecular systems were equilibrated as described above.

Water was modelled with the TIP3P[27] model, the bromide and sodium ion parameters were taken from Joung and Cheatham work.[28]

All bonds were constrained using the LINCS algorithm[29] whereas the geometry of water molecules was fixed with the SETTLE algorithm.[30] Virtual interaction sites[31] of all the hydrogen atoms were introduced to remove all the internal vibrational degree of freedom and the simulations were performed by using a time step of 4 fs.

Short-range electrostatic interactions were calculated using a cut-off of 1.2 nm and the long-range electrostatic interactions were treated by using the Particle Mesh Ewald method (PME).[32,33] The van der Waals interactions were switched off between 1.0 and 1.2 nm and the Verlet cut-off scheme[34] was used with a minimum cut-off of 1.0 nm for short-range Lennard-Jones interactions.

The temperature of nucleic acids, Gemini surfactants and water/ions was kept constant separately at 298 K using the velocity rescale method[35] with a coupling constant τ_T of 0.1 ps. The first 20 ns of each simulation were run in the *NPT* ensemble using the Berendsen barostat[36] (P = 1 bar, τ_P = 1.0 ps) after which the Parrinello–Rahman barostat[37] (P = 1 bar, τ_P = 4.0 ps) was used. Pressure coupling was applied isotropically and the periodic boundary conditions were applied in all three dimensions.

For each ODN/Gemini molecular system, we performed two independent MD simulations starting from different initial configurations obtained by the random orientation of the ODNs and Gemini micelles, in the case of monomeric complexes, and of two monomeric complexes, in the case of the dimeric complexes.

The trajectories obtained by MD simulations were analyzed with the GROMACS analysis tools, VMD 1.9.2[38] and in-house scripts, exploiting the MDAnalysis library.[39]

Results and discussion

(a) SAXS

Fig. 2 shows the typical pattern of siRNA (4.5×10^{-3} M), 12-3-12 micelles (1.25×10^{-3} M) and their complexes at charge ratios 0.75 and 1.25.

The SAXS patterns of 12-3-12 micelles were modelled using a spherical core–shell form factor with a Schulz size distribution function of the radius.[40] An additional scattering Lorentzian term was also included in order to describe the excess of scattering in the low-q region, corresponding to the structure factor of micellar clusters.[41] For the ODNs, the form factor of a cylinder with a finite size was chosen to model the scattering intensity profiles.[41]

The scattering patterns of the complexes are characterized by a quasi-Bragg peak indicating that ordered structures are already present in solution at 20 ms after mixing. We have previously shown that in such complexes, ODNs and micelles are arranged as ''sandwiches'' internally layered with a repeat distance of 3–4 nm.[13] The structural details of Gemini aggregates in water were recently investigated in depth by ESR and SAXS and are reported in ref. 42. In this study, the role played by molecular parameters (such as the spacer length) in the size and shape of micelles was elucidated. This role had been already evidenced by Karlsson *et al.*[43] and by Devinsky *et al.*,[44] who analysed differences in the compaction of long DNA filaments driven by micelles of Gemini with variable spacer extension. Another study performed by Uhríková *et al.* investigated the internal organization of lipoplexes formed by Gemini micelles and long filaments of DNA extracted from calf thymus.[45]

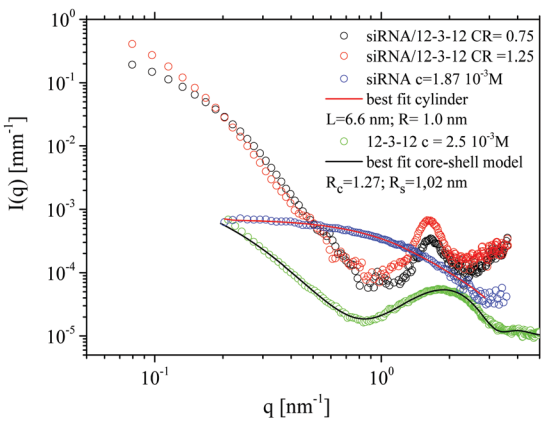

Fig. 2 SAXS intensity profiles of 12-3-12 micelles, siRNA and complexes at two different charge ratios (CR = 0.75 and CR = 1.25) recorded 20 ms after mixing. In the complex solution, the total surfactant concentration (1.25×10^{-3} M) is ~1.5 times the CMC of 12-3-12. In the reference systems siRNA is 4.5×10^{-5} M and 12-3-12 is 1.25×10^{-3} M. Solid lines are the best fitting using the polydisperse core shell (black) and cylinder-like (red) form factors, for the 12-3-12 micelles and siRNA, respectively.

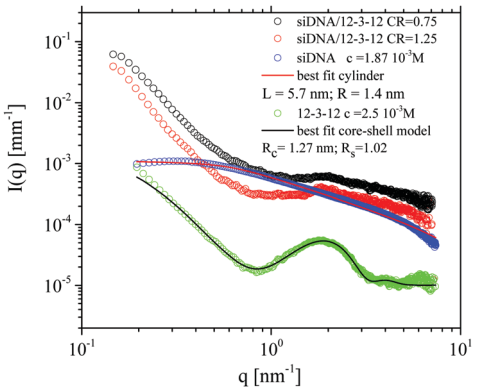

Fig. 3 SAXS intensity profiles of 12-3-12 micelles, siDNA and complexes at two different charge ratios (CR = 0.75 and CR = 1.25) recorded 20 ms after mixing. In the complex solution, the total surfactant concentration (1.25×10^{-3} M) is ~1.5 times the CMC of 12-3-12. In the reference systems siDNA is 4.5×10^{-5} M and 12-3-12 is 1.25×10^{-3} M. Solid lines are the best fitting using the polydisperse core shell (black) and cylinder-like (red) form factors, for the 12-3-12 micelles and siRNA, respectively.

The SAXS profiles of siDNA 4.5×10^{-3} M and its corresponding complexes with 12-3-12 micelles at charge ratios 0.75 and 1.25 are shown in Fig. 3. A close comparison between Fig. 2 and 3 shows that aggregates with siDNA and 12-3-12 are characterized by a Bragg peak broader than those of the corresponding siRNA/12-3-12 systems, indicating that siDNA/Gemini complexes are more loosely packed and less ordered.

A very similar trend was also observed for 12-6-12 (see the ESI,† Fig. S1 and S2). This close resemblance indicates that the internal arrangement in the complex is primarily determined by the ODN type (RNA or DNA) and weakly depends on the Gemini spacer length.

To obtain information on the size of the complexes, Tr-SAXS data at low q were analysed by using the Guinier approximation:

$$I(q) = I_0 \exp\left(-\frac{1}{3}q^2 {R_g}^2\right),$$

where I_0 is extrapolated at $q \to 0$ and R_g is the gyration radius of aggregates. Such analysis provides a lower limit estimation for the size of the aggregates since their overall size cannot be fully resolved in the available q range.

The results of the Guinier analysis are reported in Fig. 4 (A and B) for 12-3-12 and 12-6-12, respectively.

siRNA based complexes have significantly higher R_g than siDNA complexes, independently of the surfactant length of 14 to 18 nm compared to 8 to 10 nm. The size of the siRNA complexes is also more dependent on the charge ratio than the size of DNA complexes. Finally, in the time window observed, the size of the siRNA complexes tends to increase while it tends to decrease for siDNA complexes.

(b) Molecular dynamics simulations

Molecular dynamics simulations were used to investigate, at the atomic resolution, the complexation of ODN molecules with micelles of 12-3-12 and 12-6-12. We focused on the study of the interaction between Gemini surfactants and ODNs, with particular

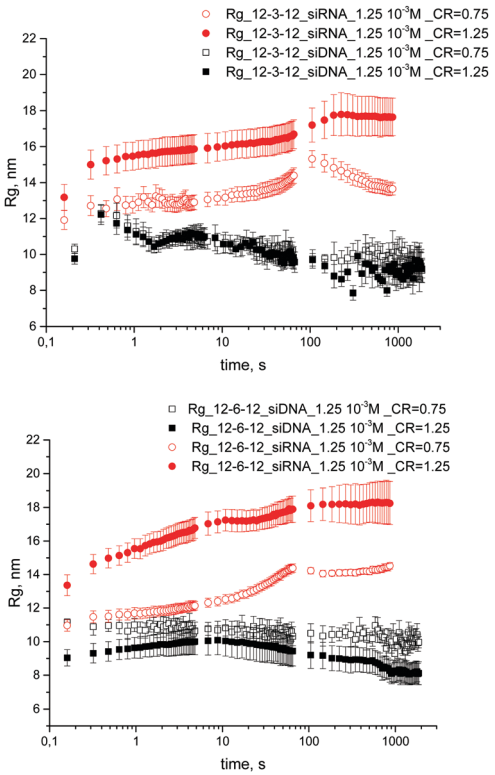

Fig. 4 Time evolution of R_g after mixing ODNs (siRNA or siDNA) with surfactants, at two different CR: 0.75 and 1.25. Panel A and B shows R_g trend for ODN/12-3-12, ODN/12-6-12 respectively.

attention paid to the role of the spacer of Gemini in the complexation processes. In fact previously reported investigations, both computational[46–48] and experimental,[49] highlighted the role of length and of the nature of the spacer in determining the properties and morphology of Gemini aggregates.

We focused our MD simulations on the study of the cationic ODN/micelle complexes with a charge ratio [−]/[+] = 0.75 for their potential as non-viral vectors of ODN biomolecules.

Here we describe first the results obtained from all-atoms MD simulations of micellar aggregates formed by 12-3-12 and 12-6-12. Then we describe the results obtained from simulations of the monomeric and dimeric ODN/Gemini complexes.

(c) Molecular dynamics simulations of 12-3-12 and 12-6-12 micelles

We simulated the aggregation of 27 molecules of 12-3-12 or 12-6-12 surfactants to form a single micelle. The aggregation number of 27 for the cationic micelles allows having, in the studies with the ODNs, the same charge ratio [−]/[+] of 0.75 used in the SAXS experiments. This aggregation number is also consistent with the data reported in the literature[42,50] for diluted solution, (close to the CMC), of these surfactants. In fact, at low concentration both the Gemini surfactants, 12-3-12 and 12-6-12, aggregate to form nearly spherical micelles with an aggregation number of about 25.

The structural parameters, obtained by the analysis of the last 20 ns of equilibrated trajectories, are reported in the ESI†

(Table S1) for 12-3-12 and 12-6-12 micelles. The micelles of 12-3-12 have a smaller average radius of gyration (R_g = 1.47 nm), then 12-6-12 micelles (R_g = 1.54 nm). This difference is mainly due to the larger size of the 12-6-12 spacer group and the polar head.

The size of single micelles can be estimated by the value of the mean distance between head groups and the micelle centre of mass. In the case of 12-3-12 and 12-6-12 the radial distribution of head groups (Fig. S2 of the ESI†) shows a maximum value of 1.77 and 1.75 nm, respectively.

The two kinds of micelles present a different organization of head groups on the surface of the aggregate. Fig. 5 shows the probability distribution of the distance (d_s) of nitrogen atoms within the same molecule. In the micelle of 12-3-12, where the spacer is short and rigid (only three methylene, n = 3), the distribution of the distance between nitrogen atoms is sharp with the maximum value at 0.51 nm (Fig. 5a). On the other hand, the micelle of 12-6-12, with a longer spacer (n = 6), shows a broader distribution with respect to 12-3-12, due to the flexibility of the spacer, with a maximum at 0.76 nm (Fig. 5b).

In order to obtain information on the reciprocal organization of Gemini molecules on the surface of the micelle, we calculated the Radial Distribution Function (RDF) for nitrogen atom pairs belonging to different surfactant molecules (Fig. 6a and b). The N–N RDF for the micelle of 12-3-12 shows a first peak at 0.86 nm, due to the first shell of neighbor nitrogen atoms, and a broader second one of similar intensity at 1.2 nm due to the second coordination shell. The inclusion of the intramolecular interaction in the calculation of RDF of nitrogen atoms is shown in the inset of Fig. 6a where the sharp and intense peak at 0.5 nm is due to the distribution of N–N pairs belonging to the same molecule. In the micelle of 12-6-12 the N–N RDF shows the first peak at 0.85 nm, similarly to what observed in the case of the 12-3-12 micelle, and a second less intense peak at 1.5 nm, due to the nitrogen atoms covalently linked to the nitrogen atoms in the first shell (Fig. 6b). The N–N RDF of 12-6-12 calculated taking into account also the intramolecular interaction between nitrogen atoms (the inset of Fig. 6b) shows the intense peak at 0.8 nm (due to the intramolecular interactions) overlapping with the peak relative to the first shell of intermolecular interactions. In the micelle of 12-3-12 the distance between nitrogen atoms presents a bimodal distribution as evidenced in the inset of Fig. 6a: a first maximum of the distribution at a short N–N distance (0.51 nm) between nitrogen atoms linked by the spacer and a second maximum at a larger distance (0.86 nm) between nitrogen atoms belonging to different surfactant molecules.

On the other hand, in the case of 12-6-12 the intramolecular distance between nitrogen atoms is similar to the intermolecular distance (0.8 nm), in this case the distribution of ammonium head groups on the surface of the aggregate is more homogeneous and similar to that of the single chain surfactants.[50] Fig. 7 reports the snapshots of 12-3-12 (a) and 12-6-12 (b) after 60 ns of MD simulations showing the head groups belonging to the same molecule in different colors (blue and red) and the spacer colored in cyan. At a glimpse, the surface of the 12-6-12 micelle features a more homogeneous distribution of head groups with respect to the 12-3-12 micelle. Furthermore, in the case of the micelle of 12-3-12 (Fig. 7a), it is possible to observe a shorter distance between head groups belonging to the same molecules with respect to the distance between head groups of different surfactant molecules, as obtained by the analysis of the N–N distance distributions.

Detailed information on the shape of the two micelles was obtained by the analysis of the principal moment of inertia (Table S1, ESI†).

For both micelles two of the three components of the principal moment of inertia have similar values, whereas the third one has a much lower value in the ratio 1 : 1.3 : 1.4 and

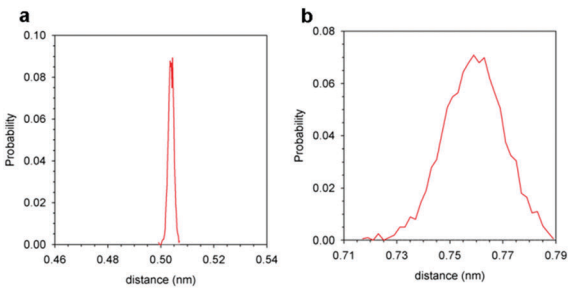

Fig. 5 Probability distribution of the average distance between nitrogen atoms within the same molecule of 12-3-12 (a) and 12-6-12 (b) surfactants.

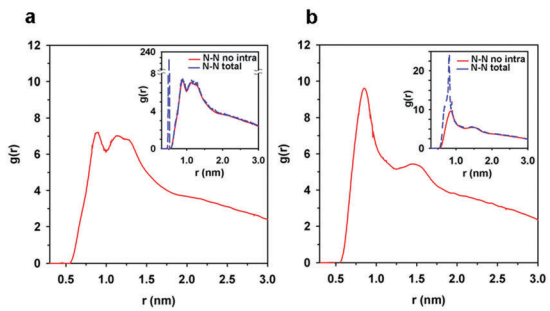

Fig. 6 Radial distribution function for intermolecular N–N pairs for 12-3-12 (a) and 12-6-12 (b) micelles. The inset shows the total (blue dashed line) as well as the mere intermolecular contribution to the N–N RDF (red line).

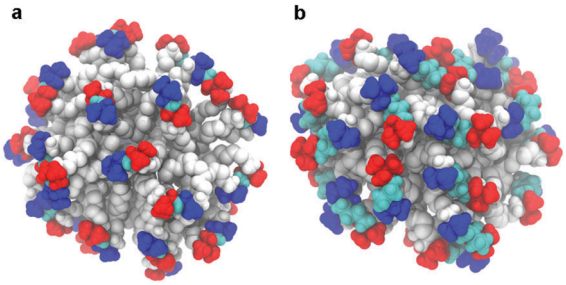

Fig. 7 Snapshot at 60 ns of MD simulations of the 12-3-12 (a) and 12-6-12 (b) micelles. Water, bromide ions and the hydrogen atoms of alkyl chains are not represented for clarity. The head groups of each Gemini surfactant are represented with different colors (blue and red) to better illustrate the head group distribution on the micellar surface. The atoms of the spacer are colored in cyan.

1 : 1.4 : 1.5 for 12-3-12 and 12-6-12 respectively, indicating a prolate ellipsoidal shape.

These results are in agreement with literature data for a diluted solution of these surfactants, for instance with the results obtained by EPR and SAXS.

(d) Molecular dynamics simulations of ODN/Gemini complexation

In order to investigate the complexation of nucleic acids with micelles of Gemini surfactants from an atomistic point of view, we started with classical molecular dynamics simulations of four molecular systems composed of one molecule of the 21 bp ODN (siRNA or siDNA) and one cationic micelle formed by 27 molecules of 12-3-12 or 12-6-12. The simulated systems allow having the ratio between the number of phosphate groups of ODNs and the number of ammonium groups of Gemini ([−]/[+]) of 0.74, close to the charge ratio used in the SAXS experiments.

For each MD simulation the initial configuration of the system was constructed by placing the centre of mass of the micelle at 4.0 nm from the centre of mass of nucleic acid. The complexation of nucleic acids by cationic micelles of 12-3-12 and 12-6-12 is driven by the electrostatic interaction between the cationic head groups of Gemini surfactants and the phosphate groups of nucleic acids.

Monitoring the temporal variation of the distance between the centre of mass of the nucleic acid and the micelle (Fig. 8) allowed following the formation of the ODN/micelle complex and obtaining information on the kinetics of complexation. For all the simulated systems such a distance decreases rapidly within the first few nanoseconds and reaches a plateau with a value of 1.6 nm as shown in Fig. 8. The association between the micelle and the nucleic acid occurs within the first 10 ns of simulations bringing to the formation of a stable complex.

It is generally accepted that complexation between nucleic acids and cationic micelles or polyelectrolytes occurs *via* two consecutive steps:[51–53] (i) the partial desolvation and subsequential removal of the counterions of both the aggregates and biomolecules and (ii) the search of their optimal interaction. This process allows obtaining the minimum value of the free energy of the molecular system. Fig. 9 shows the snapshots at different times of MD simulations of the siRNA/12-3-13 and siDNA/12-3-12 systems.

Initially, the interaction between micelles and nucleic acids involves a few molecules of surfactants. After this initial phase, the micellar aggregate optimizes the interaction with nucleic acid by changing its shape and organization. The structures of the complexes after 100 ns of MD simulations clearly evidence a different organization of the surfactant molecules bound to siDNA and siRNA.

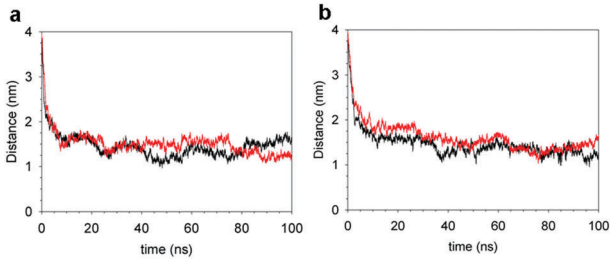

Fig. 8 Distance between the center of mass of nucleic acids and the micelles of 12-3-12 (a) and 12-6-12 (b). SiRNA/micelle system (red line), siDNA/micelle system (black line).

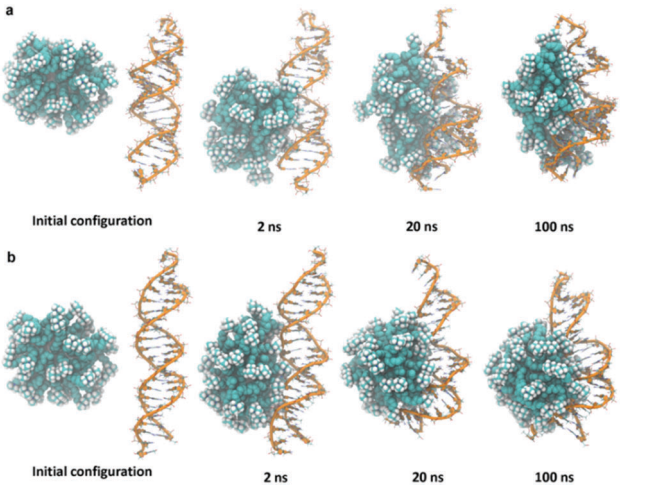

Fig. 9 Structure of the simulated systems during various steps of complexation: (a) siRNA with micelle of 12-3-12, (b) DNA and micelle of 12-3-12.

In the case of siRNA, the micelle of 12-3-12 adopts a cigar-shaped morphology and covers one of the faces of the siRNA, that is facing the micelle in order to neutralize the charges of the phosphate groups. In the complex with siDNA the micelle of 12-3-12 adopts an ellipsoidal shape and interacts only with a portion of the helix of the nucleic acid that appears slightly bent and wrapped around the micelle. On the other hand, the ODN/12-6-12 complexes show structures similar to those of ODN/12-3-12 complexes. In both cases, we observed a larger deformation of the structure of the micelle in the complex with siRNA and an ellipsoidal shape of the micelle in the complex with siDNA (Fig. S3 in the ESI†).

We also analysed the complexation process in terms of the number of close contacts between the micelle and nucleic acid. Fig. 10a and b shows the time dependence of the number of contacts between all Gemini atoms within 0.3 nm from the ODN atoms. This number increases during the complexation despite the different morphology of the helix of siDNA and siRNA and depends only on the type of surfactant (not on the nature of the nucleic acid). For the complexes siRNA/12-3-12 and siDNA/12-3-12 only a slight difference in the number of contacts was observed between 45 and 75 ns of simulation due to a temporary protrusion of the micelle into the major groove of siDNA (Fig. 10a).

To obtain detailed information on the interaction between the two components of the complex, we analysed the nature of the contacts between surfactant molecules and the atoms of nucleic acid. In Fig. 10c we reported the number of contacts between the atoms of the micelle and (i) the backbone atoms of the nucleic acid or (ii) the atoms of the bases of the nucleic acid. For all simulated systems the surfactant molecules interact primarily with the ODN backbone rather than with its bases.

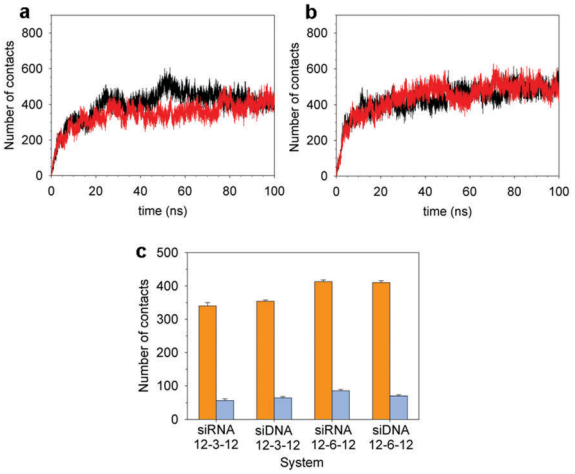

Fig. 10 Number of close contacts between ODNs and the micelle of 12-3-12 (a) and 12-6-12 (b) (number of micelle atoms within 0.3 nm from any nucleic acid atom) as a function of time. Black lines siDNA/micelle, red lines siRNA/micelle. (c) Number of contacts between all atoms of the micelle with the backbone atoms (orange) and the atoms of the bases (cyan) of the nucleic acid.

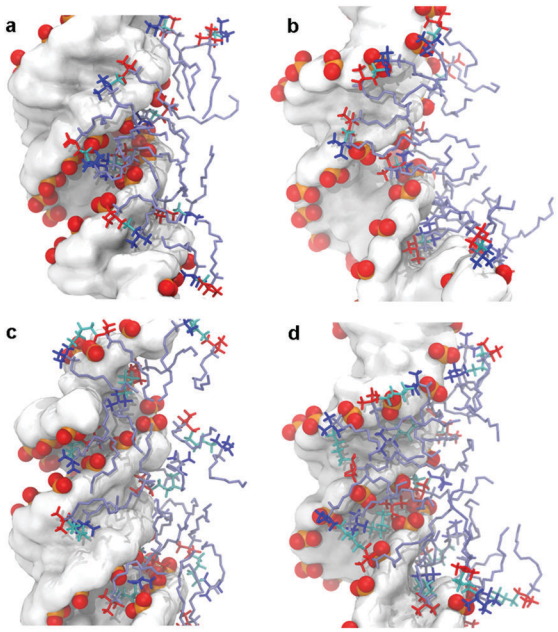

Fig. 11 Snapshots of siRNA/12-3-12 (a), siDNA/12-3-12 (b) siRNA/12-6-12 (c) and siDNA/12-6-12 (d) after 100 ns of MD simulations. The ODN molecular surface is shown in white and the phosphate groups are shown as CPK spheres (the phosphorus atoms in orange and the oxygen atoms in red). The Gemini molecules within 0.3 nm from the ODN atoms are shown in stick; the head groups are coloured in blue and red and the spacer is coloured in cyan.

The number of nitrogen/phosphorus contacts gives information on the strength of the interaction between the micelle and nucleic acid.[54] The calculated average number of nitrogen/phosphorus contacts is 28 ± 3, 20 ± 2, 28 ± 3 and 25 ± 3 for siDNA/12-3-12, siRNA/12-3-12, siDNA/12-6-12 and siRNA/12-6-12, respectively. In the complex siDNA/12-3-12 we observe a higher number of N/P contacts with respect to the complex siRNA/12-3-12. These differences can be rationalized considering the higher accessibility of phosphate groups in the B-DNA with respect to the A-RNA. In fact, as shown in Fig. 11, in B-DNA the phosphate groups are more exposed with their oxygen atoms pointing outward from the helix axis of the nucleic acid, whereas in A-siRNA the phosphate groups are less exposed, their oxygen atoms being more directed toward the minor groove of the double helix.[55] In the complexes containing the micelle of 12-6-12 we observed a similar number of N/P contacts for both ODN/micelle complexes due to a higher flexibility of the spacer in Gemini molecules. This allows a better organization of the ammonium groups around the phosphate groups (Fig. 11c and d).

The different accessibility of phosphate groups of B-DNA and A-RNA allows us to make a hypothesis on the different structure observed between the complexes siRNA/micelle and siDNA/micelle (Fig. 9). In the siRNA/micelle complexes the lower exposure of phosphate groups and the rigid structure of ODNs determine a larger reorganization of the micelle that adopts an elongated structure on the surface of the siRNA to maximize the number of N/P contacts and optimize the interaction with the ODNs. In the DNA/micelle complexes, the micelle does not need to deform its structure for obtaining the optimal interaction with DNA, due to the accessibility of phosphate groups of ODNs and the flexibility of DNA which slightly bents and wraps the aggregate.

The analysis of the nitrogen atom distribution of Gemini surfactants close to ODNs (within 0.3 nm of each atoms of nucleic acid) evidences a reorganization of the head groups on the surface of the micelle in the contact region with the biomolecule. In all ODN/12-3-12 complexes the value of the averaged intramolecular distance between nitrogen atoms of Gemini is 0.51 nm, as in the case of an isolated micelle. In the ODN/12-6-12 complexes the intramolecular distance between nitrogen atoms slightly decreases with respect to the isolated micelle of 12-6-12 (0.76 nm) with a value of 0.74 nm in siDNA/12-6-12 and 0.73 nm in siRNA/12-6-12 (Fig. S5 of the ESI†). The differences in the value of the intermolecular distance between nitrogen atoms observed in the ODN/12-6-12 complexes reflect the distance between the phosphate groups in siRNA (A-form) and siDNA (B-form). In fact, as evidenced by the RDF between phosphate groups of siRNA and siDNA (Fig. S6 of the ESI†), the distance between two adjacent phosphate groups is 0.58 nm and 0.68 nm for siRNA and siDNA, respectively. The length of the spacer of 12-6-12 allows modulating the distance between nitrogen atoms and adopting the more favorable conformation for the interaction with the phosphate groups of ODNs (Fig. 11c and d).

The reorganization of head groups in the contact region is also confirmed by the analysis of the RDF of nitrogen atoms (Fig. S7 of ESI†) of the Gemini close to the ODN surface.

In order to obtain information on the size of the monomeric complexes, we calculated the values of the radius of gyration of the complex, R_g(complex), and those of the micelle and nucleic acid within the complex, R_g(mic) and R_g(ODN), respectively.

The average values of the radius of gyration obtained from MD simulations are reported in Table 1. In the siDNA/micelle complexes the value of R_g(mic) slightly increases with respect

Table 1 Radius of gyration (R_g, nm) for ODNs, micelles and complex in complexes of ODNs (siDNA or siRNA) with micelles of Gemini 12-3-12 and 12-6-12

System	ODN	Micelle	Complex
siDNA[a]	2.15 ± 0.01		
siRNA[a]	1.90 ± 0.03		
siDNA/12-3-12	2.00 ± 0.03	1.53 ± 0.04	1.90 ± 0.04
siRNA/12-3-12	1.86 ± 0.01	1.66 ± 0.02	1.88 ± 0.01
siDNA/12-6-12	2.01 ± 0.02	1.63 ± 0.03	1.94 ± 0.01
siRNA/12-6-12	1.82 ± 0.01	1.78 ± 0.04	1.93 ± 0.01

[a] MD simulations of ODNs without micelles.

to the value obtained for the isolated micelles of 12-3-12 and 12-6-12, 1.47 and 1.57 nm respectively. In the complexes with the siDNA, the micelles of 12-3-12 and 12-6-12 deform slightly their structures with respect to the isolated aggregate maintaining substantially an ellipsoidal shape with the principal moments of inertia in the ratio 1 : 1.3 : 1.5 and 1 : 1.5 : 1.7 for the micelles 12-3-12 and 12-6-12, respectively. The value of R_g(mic) of the siRNA/micelle complexes is greater than that obtained in the complexes with siDNA and confirms the larger deformation of the micelle aggregates in these complexes due to optimisation of the interaction with siRNA.

These results highlight the peculiar features of the micellar aggregates with respect to other types of nanoparticles, such as dendrimers[56] or gold nanoparticles,[57] used for complexing nucleic acids. Dendrimers or gold nanoparticles present a more rigid structure with respect to micelles due to stronger chemical bonds (covalent and metallic bonds, respectively) joining the different parts and functional groups of nanoparticles. In the micelles, the surfactant molecules interact through non covalent bonds, *i.e.* weaker interactions, providing the flexibility to the complexes necessary to adopt the most favourable shape and organization.

(e) Dimeric complexes

The structure of the ODN/micelle obtained by MD simulations highlights an asymmetrical neutralization of the ODN charges by the interaction with Gemini aggregates. This asymmetrical neutralization is responsible for the assembly of different complexes to form the large aggregates (15–20 nm) evidenced by the SAXS results. In order to obtain structural information on the aggregates containing various units of the ODN/micelle complex, we studied the aggregation of two units of ODN/micelle for the four systems siRNA/12-3-12, siDNA/12-3-12, siRNA/12-6-12 and siDNA/12-6-12.

Fig. 12 shows the structures obtained for the dimeric complexes containing two molecules of ODNs and two micelles of Gemini after 100 ns of MD simulations. The dimeric complexes containing siRNA appear more compact and more ordered with respect to DNA complexes in agreement with the SAXS results.

The averaged radius of gyration listed in Table 2 confirms the formation of a more compact architecture for the siRNA with respect to siDNA.

In the aggregates formed by two ODN/micelle complexes, the ODNs and the micelles are organised in a "sandwich" like structure in which ODNs and micelles are alternately layered. The intermicellar distances, calculated by the distance between the centre of mass of two micelles in the dimeric complexes, are

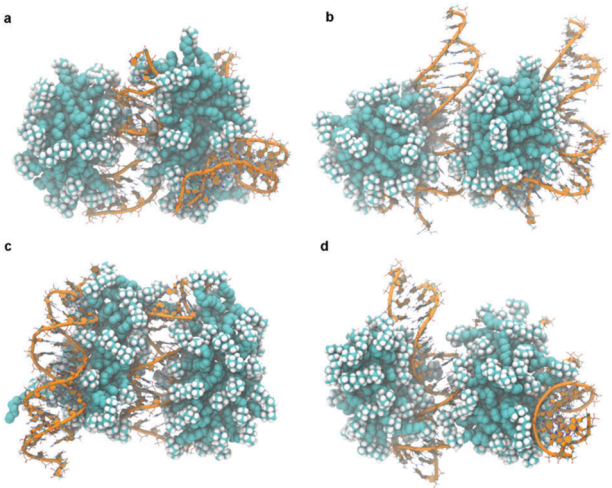

Fig. 12 Structure of the dimeric complexes of (a) siRNA/12-3-12, (b) siDNA/12-3-12, (c) siRNA/12-6-12 and (d) siDNA/12-6-12 after 100 ns of MD simulations.

Table 2 Gyration radius (R_g, nm) of ODNs, micelles and complexes in dimeric complexes of ODNs (siRNA or siDNA) for 12-3-12 and 12-6-12 Gemini. The intermicellar distance (d(mic), nm) is taken between the centre of mass of two micelles in dimeric complexes

System	ODN	Micelle	Complex	d(mic)
siDNA/12-3-12	1.96 ± 0.01 1.95 ± 0.02	1.59 ± 0.04 1.57 ± 0.01	2.68 ± 0.02	3.80 ± 0.03
siRNA/12-3-12	1.75 ± 0.03 1.83 ± 0.01	1.59 ± 0.03 1.63 ± 0.02	2.50 ± 0.01	3.48 ± 0.04
siDNA/12-6-12	1.93 ± 0.01 2.01 ± 0.02	1.67 ± 0.02 1.67 ± 0.03	2.75 ± 0.03	3.77 ± 0.02
siRNA/12-6-12	1.82 ± 0.01 1.84 ± 0.02	1.65 ± 0.01 1.72 ± 0.01	2.65 ± 0.01	3.57 ± 0.06

reported in Table 2. For the complexes containing siRNA, we observed a lower intermicellar distance due to the flattened morphology of the micelle arranged between the ODNs compared to the complexes with DNA. The values of the intermicellar distance obtained from MD simulations are in agreement with the values of the repeat distance obtained by SAXS experiments (3–4 nm). This difference in final packing can be related to the difference of deformation observed in the 1 : 1 complex. It was observed that surfactant micelles were more prone to get anisotropic when complexed with RNA than when complexed with DNA. As a result, and because cylinders pack at a higher volume fraction (92%) than spheres (74%), the 2 : 2 complex with RNA is more compact.

Conclusions

Non-viral carriers for siRNA delivery are widely investigated in gene therapy research as a safer alternative to viral vectors. However, the transfection efficacy of complexes between synthetic vectors and genetic material still remains too low for envisaging extensive use. Thus, deeper knowledge of the structure and functioning of these complexes at the molecular level should be beneficial to understand, and possibly improve, their performance.

Comparatively few studies in current literature deal with short DNA fragments, which are also interesting both for theoretical reasons and biomedical applications. The comparison between siRNA and siDNA is subtle and can be addressed only by high resolution methods. In this paper we compared the physico-chemical properties of RNA and DNA oligonucleotides complexed with micelles of Gemini surfactants by combining Tr-SAXS measurements and MD simulations.

While Tr-SAXS provides information on the size and shape of the complexes at the intermediate-long time scale (from 10–20 millisecond to several minutes), MD simulations are able to give atomistic details at the first instants after the component assembly (from 10 to 100 ns).

Some of the most relevant results are the following:

(i) SAXS and MD both show that the complexes formed by siRNA are more ordered and tightly packed than their siDNA counterparts;

(ii) the structures of dimeric complexes ODN/micelle obtained by MD simulations are in agreement with the sandwich structure (alternate layers of micelles and ODNs), previously found for the system siRNA/Gemini with SAXS experiments;

(iii) the intermicellar distances in the dimeric complexes obtained by MD simulations are in agreement with the values of the repeat distance obtained from the SAXS experiments.

Therefore, the ensemble of the results extracted from techniques which probe different time scales indicate that the internal structure assumed at the very first nanoseconds is basically maintained afterwards. From the mechanistic point of view such findings allow us to visualize the process of complex formation as a squeezing of Gemini micelles between the harder molecules of double strand ODNs, but can be also profitably used to establish application protocols. In fact the present study confirms the spontaneous and quick formation of stable complexes, thus allowing easy preparation *in situ* prior to use. The observed stability also suggests that during standard times required for administration the complex integrity is guaranteed. Moreover, the number of contact analysis indicates that complexes with 12-6-12 are more stable than those with 12-3-12, while this latter surfactant has a slightly higher affinity for siDNA rather than siRNA.

Although our all-atoms MD simulations were performed on ODN/Gemini complexes of limited size with respect to the complexes observed by SAXS experiments, the results obtained by computational and experimental investigations are in good agreement. Further, the atomistic analysis performed in this study is the fundamental basis for the simulation of larger aggregates and longer times (~milliseconds) similar to the time scale of Tr-SAXS. This time scale can be accessed by coarse grained MD simulations, to obtain insights into the structure and organization of more extended complex systems.

Acknowledgements

The authors are indebted with the ESRF for beamtime allocation at the ID02 beamline and with Dr Michael Sztucky for expert assistance.

References

1 A. K. Leung, Y. Y. Tam and P. R. Cullis, *Adv. Genet.*, 2014, **88**, 71–110, DOI: 10.1016/B978-0-12-800148-6.00004-3.
2 S. M. Elbashir, J. Harborth, W. Lendeckel, A. Yalcin, K. Weber and T. Tuschl, *Nature*, 2001, **411**, 494–498.
3 A. Fire, S. Xu, M. K. Montgomery, K. A. Kostas, S. E. Driver and C. C. Mello, *Nature*, 1998, **391**, 806–811.
4 S. M. Elbashir, J. Harborth, W. Lendeckel, A. Yalcin, K. Weber and T. Tuschl, *Nature*, 2001, **24**, 411(6836), 494–498.
5 J. C. Burnett, J. J. Rossi and K. Tiemann, *Biotechnol. J.*, 2011, **6**, 1130–1146.
6 M. Quanz, D. Chassoux, N. Berthault, C. Agrario, J. S. Sun and M. Dutreix, *PLoS One*, 2009, **4**(7), e6298, 10.1371/journal.pone.0006298.
7 M. Quanz, N. Berthault, C. Roulin, M. Roy, A. Herbette, C. Agrario, C. Alberti, V. Josserand, J. L. Coll, X. Sastre-Garau, J. M. Cosset, L. Larue and J. S. Sun, *Clin. Cancer Res.*, 2009, **15**(4), 1308–1316, DOI: 10.1158/1078-0432.CCR-08-2108.
8 F. Devun, G. Bousquet, J. Biau, A. Herbette, C. Roulin, F. Berger, J. S. Sun, S. Robine and M. Dutreix, *J. Gastroenterol.*, 2012, **47**(3), 266–275, DOI: 10.1007/s00535-011-0483-x.
9 K. T. Shum and J. J. Rossi, *Adv. Genet.*, 2015, **89**, 153–177, DOI: 10.1016/bs.adgen.2014.10.004.
10 G. Candiani, *Non-Viral Gene Delivery Vectors Methods and Protocols*, Springer, 2016.
11 K. Gupta, K. A. Afonin, M. Viard, V. Herrero, W. Kasprzak, I. Kagiampakis, T. Kim, A. Y. Koyfman, A. Puri, M. Stepler, A. Sappe, V. N. Kewal Ramani, S. Grinberg, C. Linder, E. Heldman, R. Blumenthal and B. A. Shapiro, *J. Controlled Release*, 2015, **213**, 142–151.
12 C. Bombelli, S. Borocci, M. Diociaiuti, F. Faggioli, L. Galantini, P. Luciani, G. Mancini and M. G. Sacco, *Langmuir*, 2005, **21**, 10271–10274.
13 S. Falsini, S. Ristori, L. Ciani, E. Di Cola, C. T. Supuran, A. Arcangeli and M. In, *Soft Matter*, 2014, **10**(13), 2226–2233.
14 E. H. Lee, M. Sotomayor, G. Comellas and K. Schulten, *Structure*, 2009, **17**, 1295–1306.
15 J. R. Perilla, B. C. Goh, C. K. Cassidy, B. Liu, R. C. Bernardi, T. Rudack, H. Yu, Z. Wu and K. Schulten, *Curr. Opin. Struct. Biol.*, 2015, **31**, 64–74.
16 S. A. Adcock and J. A. McCammon, *Chem. Rev.*, 2006, **106**, 1589–1615.
17 G. M. Pavan, *ChemMedChem*, 2014, **9**, 2623–2631.
18 J. A. Nash, A. Sigh, N. K. Li and Y. G. Yingling, *ACS Nano*, 2015, **9**, 12374–12382.
19 N. Kasyanenko, L. Lysyakova, R. Ramazanov, A. Nesterenko, I. Yaroshevich, E. Titov, G. Alexeev, A. Lezov and I. Unksov, *Biopolymers*, 2015, **103**, 109–112.
20 T. Kim, K. A. Afonin, M. Viard, A. Y. Koyfman, S. Sparks, E. Heldman, S. Grinberg, C. Linder, R. P. Blumenthal and B. A. Shapiro, *Mol. Ther. – Nucleic Acids*, 2013, **2**, e80, DOI: 10.1038/mtna.2013.5.
21 S. Ristori, L. Ciani, G. Candiani, C. Battistini, A. Frati, I. Grillo and M. In, *Soft Matter*, 2012, **8**, 749–756.

22 S. Pronk, S. Pall, R. Schulz, P. Larsson, P. Bjelkmar, R. Apostolov, M. R. Shirts, J. C. Smith, P. M. Kasson, D. van der Spoel, B. Hess and E. Lindahl, *Bioinformatics*, 2013, **29**, 845–854.
23 K. Hart, N. Foloppe, C. M. Baker, E. J. Denning, L. Nilsson, Jr. and A. D. MacKerell, *J. Chem. Theory Comput.*, 2012, **8**, 348–362.
24 E. J. Denning, U. D. Priyakumar, L. Nilsson, Jr. and A. D. MacKerell, *J. Comput. Chem.*, 2011, **32**, 1929–1943.
25 S. Lee, A. Tran, M. Allsopp, J. B. Lim, J. Hénin and J. F. Klauda, *J. Phys. Chem. B*, 2014, **118**, 547–556.
26 T. J. Macke and D. A. Case, Modeling unusual nucleic acid structures, in *Molecular Modeling of Nucleic Acids*, ed. N. B. Leontes and J. SantaLucia, Jr., American Chemical Society, Washington, DC, 1998, pp. 379–393.
27 W. L. Jorgensen, J. Chandrasekhar, J. D. Madura, R. W. Impey and M. L. Klein, *J. Chem. Phys.*, 1983, **79**, 926–935.
28 I. S. Joung and T. E. Cheatham, *J. Phys. Chem. B*, 2008, **112**, 9020.
29 B. Hess, H. Bekker, H. J. C. Berendsen and J. G. E. M. Fraaije, *J. Comput. Chem.*, 1997, **18**, 1463–1472.
30 S. Miyamoto and P. A. Kollman, *J. Comput. Chem.*, 1992, **13**, 952–962.
31 K. A. Feenstra, B. Hee and H. J. C. Berendsen, *J. Comput. Chem.*, 1999, **20**, 786–798.
32 T. Darden, D. York and L. Pedersen, *J. Chem. Phys.*, 1993, **98**, 10089–10092.
33 U. Essmann, L. Perera, M. L. Berkowitz, T. Darden, H. Lee and L. G. Pedersen, *J. Chem. Phys.*, 1995, **103**, 8577–8593.
34 L. Verlet, *Phys. Rev.*, 1967, **159**, 98–103.
35 G. Bussi, D. Donadio and M. Parrinello, *J. Chem. Phys.*, 2007, **126**, 14101–14107.
36 H. J. C. Berendsen, J. P. M. Postma, W. F. van Gunsteren, A. Di Nola and J. R. Haak, *J. Chem. Phys.*, 1984, **81**, 3684–3690.
37 M. Parinello and A. Rahman, *J. Appl. Phys.*, 1981, **52**, 7182–7190.
38 W. Humphrey, A. Dalke and K. Schulten, *J. Mol. Graphics*, 1996, **14**(1), 33–38.
39 N. Michaud-Agrawal, E. J. Denning, T. B. Woolf and O. Beckstein, *J. Comput. Chem.*, 2011, **32**, 2319–2327, DOI: 10.1002/jcc.21787.
40 M. Kotlarchyk and S. H. Chen, *J. Chem. Phys.*, 1983, **79**, 2461.
41 P. W. Schmidt, in *Modern Aspects of Small Angle Scattering*, ed. H. Brumberger, Kluwer Academic, Dordrecht, 1995.
42 S. Falsini, L. Ciani, A. Arcangeli, E. Di Cola, F. Spinozzi and S. Ristori, *Colloids Surf., A*, 2015, **472**, 101–108.
43 L. Karlsson, M. C. P. van Eijk and O. Söderman, *J. Colloid Interface Sci.*, 2002, **252**, 290–296.
44 F. Devínsky, M. Pisárčik and I. Lacko, *Gen. Physiol. Biophys.*, 2009, **28**, 160–167.
45 D. Uhríková, I. Zajac, M. Dubničková, M. Pisárčik, S. S. Funari, G. Rappc and P. Balgavý, *Colloids Surf., B*, 2005, **42**, 59–68.
46 E. Khurana, S. O. Nielsen and M. L. Klein, *J. Phys. Chem. B*, 2006, **110**, 22136–22142.
47 R. Wu, M. Deng, B. Kong and X. Yang, *J. Phys. Chem. B*, 2009, **113**, 15010–15016.
48 J. A. S. Almeida, E. F. Marques, A. S. Jurado and A. A. C. C. Pais, *Phys. Chem. Chem. Phys.*, 2010, **12**, 14462–14476.
49 C. Bello, C. Bombelli, S. Borocci, P. di Profio and G. Mancini, *Langmuir*, 2006, **22**, 9333–9338.
50 D. Danino, Y. Talmon and R. Zana, *Langmuir*, 1995, **11**, 1448–1456.
51 K. Wagner, D. Harries, S. May, V. Kahl, J. O. Radler and A. Ben-Shaul, *Langmuir*, 2000, **16**, 303–306.
52 E. Pozharski and R. C. MacDonald, *Biophys. J.*, 2003, **85**, 3969–3978.
53 J. Ziebarth and Y. Wang, *Biophys. J.*, 2009, **97**, 1971–1983.
54 V. Vasumathi and P. K. Maiti, *Macromolecules*, 2010, **43**, 8264–8274.
55 W. Saenger, *Principles of Nucleic Acid Structure*, Springer-Verlag, New York, 1984.
56 N. Bidisha and P. K. Maiti, *J. Phys. Chem. B*, 2011, **115**, 217–230.
57 S. K. Mudedla, E. R. A. Singam, K. Balamurugan and V. Subramanian, *Phys. Chem. Chem. Phys.*, 2015, **17**, 30307–30317.